Hindawi Publishing Corporation
Journal of Nanomaterials
Volume 2013, Article ID 613102, 14 pages
http://dx.doi.org/10.1155/2013/613102

Research Article

Manufacturing of Nanostructured Rings from Previously ECAE-Processed AA5083 Alloy by Isothermal Forging

C. J. Luis, D. Salcedo, J. León, I. Puertas, J. P. Fuertes, and R. Luri

Mechanical, Energetics, and Materials Engineering Department, Public University of Navarre, Campus de Arrosadia s/n, 31006 Pamplona, Spain

Correspondence should be addressed to I. Puertas; inaki.puerta@unavarra.es

Received 16 April 2013; Revised 1 July 2013; Accepted 1 July 2013

Academic Editor: Sheng-Rui Jian

The manufacturing of a functional hollow mechanical element or ring of the AA5083 alloy previously equal channel angular extrusion (ECAE) processed, which presents a submicrometric microstructure, is dealt with. For this purpose, the design of two isothermal forging dies (preform and final shape) is carried out using the design of experiments (DOE) methodology. Moreover, after manufacturing the dies and carrying out tests so as to achieve real rings, the mechanical properties of these rings are analysed as well as their microstructure. Furthermore, a comparison between the different forged rings is made from ECAE-processed material subjected to different heat treatments, previous to the forging stage. On the other hand, the ring forging process is modelled through the use of finite element simulation in order to improve the die design and to study the force required for the isothermal forging, the damage value, and the strain the material predeformed by ECAE has undergone. With this present research work, it is intended to improve the knowledge about the mechanical properties of nanostructured material and the applicability of this material to industrial processes that allow the manufacturing of functional parts.

1. Introduction

Severe plastic deformation (SPD) processes constitute a novel alternative for the attainment of material accumulating high values of strain ($\varepsilon \gg 1$). To this end, over the past few years, there have been a large number of studies dealing with the modification of mechanical properties and microstructure achieved in the material when accumulating this deformation level [1, 2]. Specifically, the equal channel angular extrusion (ECAE) is a discontinuous SPD process which was firstly developed by Segal in the former Soviet Union [3]. This process consists in exerting a compression force to a material through a die with two channels of, approximately, the same cross-section which intersect at an angle between 90° and 120°. Since then, this process has been deeply studied with respect to the improvement in the mechanical properties of the processed materials [1] and also with respect to the dies employed in the process [4, 5]. In research works by [6, 7], the AA5083 alloy material is processed, thus achieving an improvement in mechanical properties such as yielding point and mechanical strength (as opposed to a loss of ductility) and a reduction in the grain size down to a submicrometric level. Among the most important characteristics of SPD materials, could be mentioned the possibility of obtaining better fatigue behaviour as well as an improvement in ductility and mechanical strength [1]. In the case of nanostructured materials, the microstructure and more specifically the grain size play a very important role in the deformation and in the fracture behaviour. At the beginning of the crack, there is a strong interaction between dislocation emission and crack propagation, which is mainly influenced by the microstructure [8].

Nevertheless, the industrial applications of the aforesaid materials are not so numerous nowadays, and the number of research works that deal with the applicability of these materials is very scant. Among these studies, one can underline the research work by Zhu et al. [9], in which these authors divide the applications of these materials into two categories: those requiring a reduction in weight and good mechanical properties and those facilitating easier manufacturing in subsequent processes. On the other hand, for certain applications, material in massive form is required,

and therefore the scaling of this process is fundamental for its use in industrial applications so that one can change from processing billets of small size into processing large blocks, as is found in the study by Ferrasse et al. [10]. This research work shows the scaling of the process in such a way that they are able to obtain starting material parts processed by ECAE of 33 kg (in the case of aluminium) and 110 kg (in the case of copper).

Most of the technical papers referring to subsequent processes of ECAE processed materials deal with the study of compression tests between plane-shape dies. Some of the aluminium alloys employed in these aforesaid research works are AA1050 [11] and AA6082 [12], where in both cases the anisotropy and the hardening of the material were studied. In order to analyse the forgeability of AA5083 after ECAE processing, compression tests were performed in [13]. One of the conclusions of this research work is the improvement in the forgeability of the ECAE-processed samples. With respect to the manufacturing of parts from previously ECAE-processed materials, one of the most commonly analysed manufacturing process in the bibliography is the forging of bolts [14]. For instance, Choi et al. [15] carried out the ECAE processing of the AA1050 alloy studying its subsequent forging process through compression tests. After performing these tests, a series of bolts are manufactured by means of three forging stages and the machining of the thread. These authors observe an increase of 12% in the hardness of the head and an increase of 45% in the hardness of the bolt body. In addition, they observe an increase of 200% in the yielding point of the bolts manufactured with nanostructured material. Another interesting study is that by Yanagida et al. [16], where cold forging is applied to the manufacturing of M1.6 bolts for four different steels. The aim of these latter authors is to compare the forgeability of the materials after having been ECAE-processed and cold-rolled. The main conclusion is that the ECAE processed materials achieve a better forgeability than those rolled, although they reduce their ductility as opposed to the nondeformed material.

Among the studies manufacturing other types of parts from nanostructured material, it is relevant to cite that by Chaudhury et al. [17], in which annealed AA6061 is ECAE processed, and, subsequently, it is forged leading to a reduction of 50% in the flash, thus giving as a consequence a reduction of 10% in the required starting material and a decrease in the optimum forging temperature from 490°C to 315°C as opposed to the non-ECAE processed material. All these improvements are based on the reduction in material and energy costs for the industry field. The forging of more complex parts has been treated in research work by Lee et al. [18]. In this study, an impeller of the AZ31 magnesium alloy previously ECAE processed is hot forged. The authors perform a new die design which allows an optimum filling of the die to be obtained along with the nanostructured material. Some other advantages are a lesser amount of flash and a result closer to the desired final shape. In order to reach the optimum forging conditions, thermal stability studies are carried out at different temperature and strain rate values, concluding that the optimum forging temperature is 300°C and that the strain rate should be controlled at a range close to $0.001\,s^{-1}$. The research work by Puertas et al. [19] proposes the manufacturing of Francis blades from nanostructured AA1050 alloy. A comparison of both mechanical properties and microstructure of the manufactured blades is made between ECAE- and non-ECAE-processed materials, where an improvement in the mechanical properties of the blades manufactured from nanostructured material is observed.

In this present study, isothermal forging was selected as the deformation process subsequent to ECAE due to the fact that it is possible to obtain parts with improved mechanical properties and a lesser material cost if the process is well designed. Moreover, with the isothermal forging, a better control of the forged part microstructure is achieved thanks to the temperature control during the process [20].

In the same way as in the manufacturing of real parts from nanostructured material, the number of research works that combine finite element simulations and isothermal forging of nanostructured material is scant [21]. Among them, in the research work by Salcedo et al. [22], a series of finite element simulations of gears with different geometries are proposed to be isothermally forged at several temperature values from nanostructured material. The authors propose two possible forging die designs, and they compare the results obtained in both cases. The nanostructured starting material is assumed to be modelled with a flow rule obtained from compression tests at different temperature values over previously ECAE-processed material.

In this present study, the design and the manufacturing of forging dies are carried out for the isothermal forging of rings from nanostructured material. Diverse models of the forging process by finite element simulation are proposed. The properties of the real rings manufactured from ECAE processed materials are analysed, and these are compared with the results obtained from the finite element simulations.

The results presented in this piece of research work are based on the manufacturing procedure proposed in the Spanish Patent P201330404 by Luis et al. [23].

2. Design and Manufacturing of the Dies

In this section, the design process of the isothermal forging dies is explained as well as their manufacturing and the forging tests carried out to obtain the rings from nanostructured material.

2.1. Planning and Optimisation of the Design. The design of the dies is carried out combining design of experiments (DOE) through the use of the Statgraphics Centurion XVI software and finite element simulation employing the Simufact 11.0 software. The simulations are performed at temperature and different geometries are employed for the preform. The flow rule of AA5083 as a function of temperature (see Figure 1) has been assessed from temperature compression tests of billets ECAE processed twice using route C.

The room temperature is contemplated to be 20°C for all the cases taken into consideration, where the initial temperature of both the billet and the dies is the same as that for the isothermal forging temperature. Although

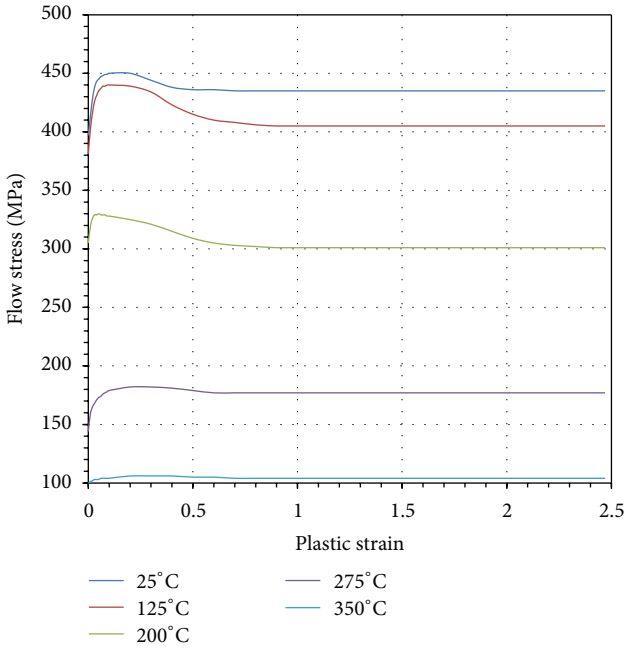

Figure 1: Flow rule of AA5083 as a function of temperature.

the heat generation for the plastic deformation depends on the strain rate, in these simulations, it has been taken as a constant with a value of 0.9. Moreover, the heat transference values due to natural convection depend on temperature, and thus the default table for natural or slightly forced convection given by the software has been selected. The heat transference values between the dies and the billet depend on the contact pressure, but it has been taken as a constant with a value of 20 kW/m^2 K.

With respect to the employed meshing, initially 7500 tetrahedral elements are taken with four integration points and an edge size of 1 mm. Curved surfaces are achieved to have elements down to an edge size of 0.25 mm so as to get a geometry closer to reality. Coarsening factor option of 1.5 is selected to decrease the number of elements at the inner part of the billet. The remeshing employed takes place at 25%, 50%, and 75% of the simulation and when distorted elements appear having a size a 15% longer than other. The friction model selected is of type Shear with a constant value of 0.1. The stroke of the upper die is 25 mm for the first forging stage and 16 mm for the second stage. Lastly, the results of force, strain and damage (following the Cockroft-Latham criterion) are compared using the design of experiments so as to select the optimum geometry.

2.1.1. Design of Experiments of the Preform Die. The forging first stage corresponds with the forming of the preform whereas the second stage corresponds with the forming of the final ring. Figure 2 shows the cross-sections of both forging dies used: the preform die (Figure 2(a)) and the ring die (Figure 2(b)). The preform die section has a geometry with fixed values and other values to be modified and studied with the DOE. These values are the following ones: draft angle (α), flash thickness (e) and fillet radii (r), where these are named as design factors for the factorial design 2^3.

This factorial design along with the central point allows us to determine the influence and the importance of these design factors over the selected response variables: forging force, damage imparted to the material and billet strain. Table 1 shows the attained results. The optimal geometry selected corresponds to a draft angle (α) of 15°, a flash thickness (e) of 3 mm, and fillet radii (r) of 2.5 mm. With the previously mentioned geometry, the maximum force value obtained is 750 kN with a maximum damage value of 0.125 and a maximum strain value of 1.4 in the preform.

The results given by the design of experiments are summarised through the Pareto chart and the estimated response surfaces. The length of each bar is proportional to the standardized effect, which is the estimated effect divided by its standard error. The vertical line can be used to judge which effects are statistically significant where any bar which extends beyond the line corresponds to an effect which is statistically significant at a confidence level of 95.0%.

As can be observed in Figure 3(a), the force required for the isothermal forging of the preform decreases when increasing the fillet radii value, the flash thickness, and the draft angle. The most influential factors are, in decreasing order, fillet radii and draft angle. Moreover, as can be observed in Figure 3(b), the damage imparted to the material decreases when increasing the fillet radii value, the flash thickness, and the draft angle, although none of the factors is statistically significant. Lastly, Figure 3(c) shows how the preform maximum strain decreases when the fillet radii value and draft angle increase and when flash thickness decreases. The only statistically significant factor is the fillet radius.

2.1.2. Design of Experiments of the Final Ring Die. The forging second stage corresponds with the forming of the ring. For this purpose, we start from the previously forged preform. The cross-section that can be observed in Figure 2(b) is that employed for the ring die, where, as in the previous case, this has a geometry with fixed values and other variable values that will be analysed by DOE. These values are as follows: draft angle (α) and fillet radii (r). In this way, the factorial design to be used is a 2^2 with one central point.

In the same way as in the design of experiments for the preform, the response variables selected are as follows: forging maximum force, maximum damage imparted to the material, and ring strain at its central zone. The obtained results can be observed in Table 2. The selected geometry corresponds to a draft angle (α) of 15° and fillet radii (r) of 1.5 mm. With this particular geometry, the maximum force value is 1100 kN with a maximum damage value of 0.175 and a maximum strain value at the ring central part of 0.7.

Figure 4(a) shows the force required for the isothermal forging of the ring, where this decreases when draft angle is increased, and it remains constant when fillet radii are varied. As can be observed in Figure 4(b), the damage imparted to the material increases when fillet radii and draft angle are increased, where it is draft angle whose influence is the most important one. Figure 4(c) shows how the strain at the

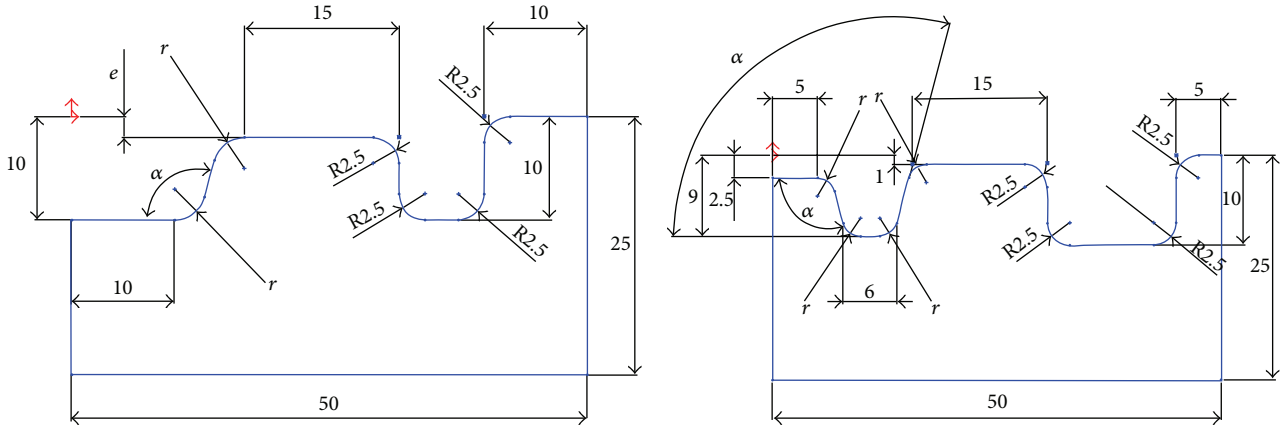

(a) Design factors for the DOE of the preform die, where the dimensions are expressed in mm

(b) Design factors for the DOE of the ring die, where the dimensions are expressed in mm

Figure 2: Design factors for the design of experiments.

Table 1: Design factors and response variables for the preform DOE, where the values in bold correspond to the optimal geometry selected.

Draft angle α (°)	Flash thickness e (mm)	Fillet radii r (mm)	Force (kN)	Damage	Strain
10	2	1.5	1815	0.25	1.7
20	2	1.5	1360	0.1	1.5
10	4	1.5	825	0.15	1.6
20	4	1.5	720	0.1	1.7
10	2	3	990	0.1	1.3
20	2	3	500	0.15	1.2
10	4	3	580	0.1	1.3
20	4	3	440	0.15	1.2
15	3	2.25	825	0.1	1.5
15	**3**	**2.5**	**750**	**0.125**	**1.4**
15	*3*	*3*	*600*	*0.125*	*1.2*
15	*4*	*3*	*520*	*0.125*	*1.2*

ring central part decreases when fillet radii and draft angle are increased, where draft angle turns out to be the most influential of both once again.

2.2. Manufacturing of the Nanostructured Ring. In this section, the attainment of the final ring through its manufacturing process is outlined. The starting material is as-cast AA5083 which is turned into billets of 90 mm in length and 20 mm in diameter. These billets are ECAE processed twice using route C in the ECAE hydraulic press shown in Figure 5(a). The set of dies employed can be observed in Figure 5(b), where these ECAE dies have an intersection angle between channels of 90° and fillet radii of 4 mm which are tangential to the entrance and exit channels.

After this process, the billets are machined into the following dimensions: 19 mm in diameter and 43 mm in length. These billets are subjected to thermal treatments in order to carry out different tests. After these heat treatments, the billets are subjected to a first isothermal forging stage, and subsequently, after the removal of the remaining flash, they are subjected to the second isothermal forging.

The isothermal forging is performed in a press with a capacity of 3000 kN, as can be observed in Figure 6(a). The dies manufactured to carry out the forging process are shown in Figure 6(b). The forging stages are carried out at a constant press velocity of 50 mm/min. Figure 7 shows the rings manufactured from previously ECAE processed materials at different temperatures values.

3. Finite Element Simulation of Mechanical Components

In the present section, the isothermal forging process of the ring with two stages is analysed. Due to the ring geometry, all the simulations performed are axisymmetric, where the x-axis is axisymmetric axis. These FEM simulations were performed by using MSC.Marc FEM Software.

The die geometry corresponds with the optimum die design previously calculated through design of experiments. Both the billet and the die are considered to behave as deformable bodies. A 2D element with an edge size of 0.5 is used for the starting billet whereas the dies are meshed

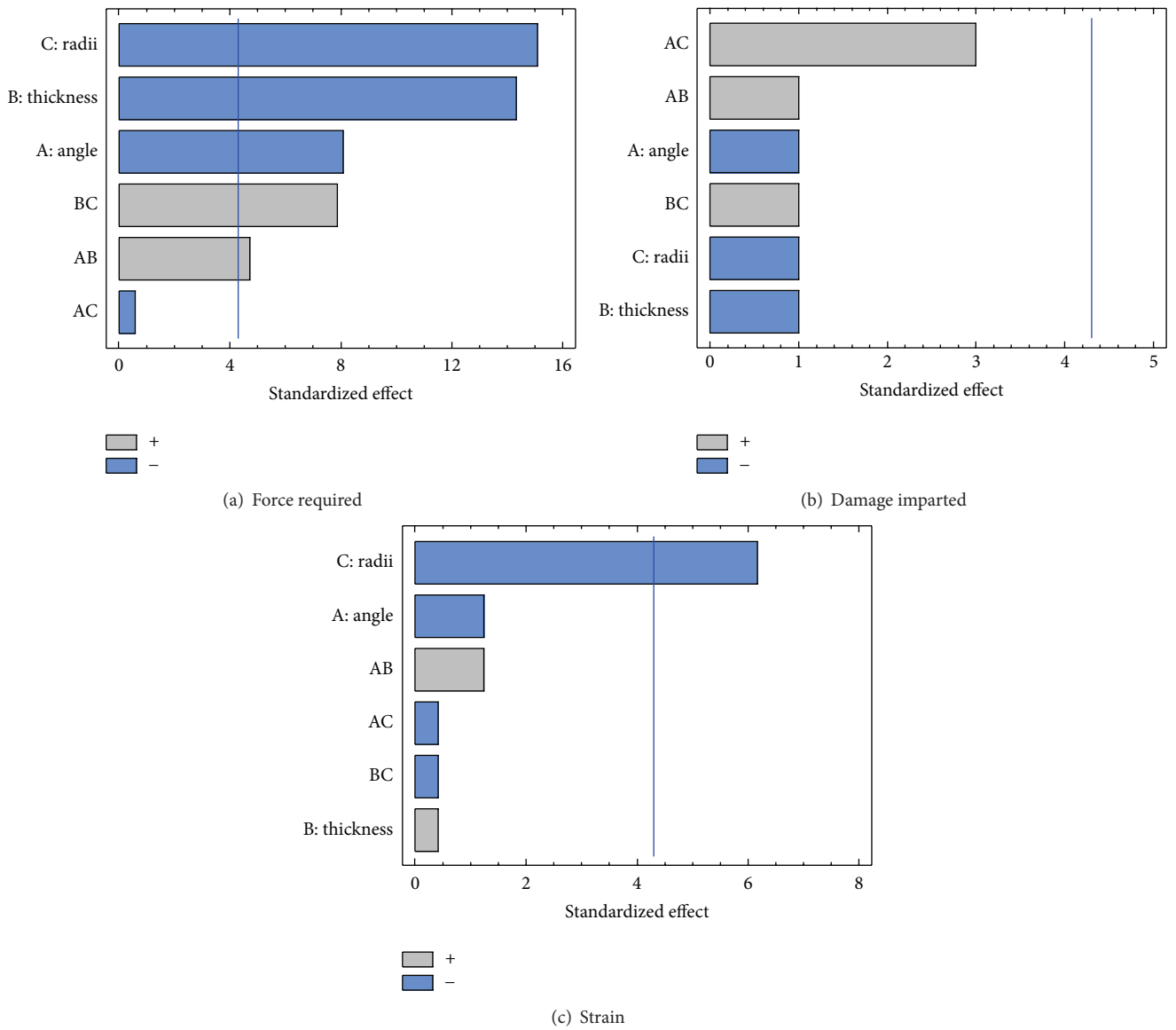

Figure 3: Pareto charts, where the bars in blue colour mean negative influence and the bars in grey colour mean positive influence on the design factors.

Table 2: Design factors and response variables of the design of experiments for the ring, where the values in bold correspond to the selected geometry.

Draft angle α (°)	Fillet radii r (mm)	Force (kN)	Damage	Strain
10	1.5	1550	0.15	1
20	1.5	290	0.2	0.3
10	3	1350	0.175	0.8
20	3	480	0.25	0.4
15	2.25	1100	0.2	0.7
15	**1.5**	**1100**	**0.175**	**0.7**
15	*2*	*1100*	*0.2*	*0.7*

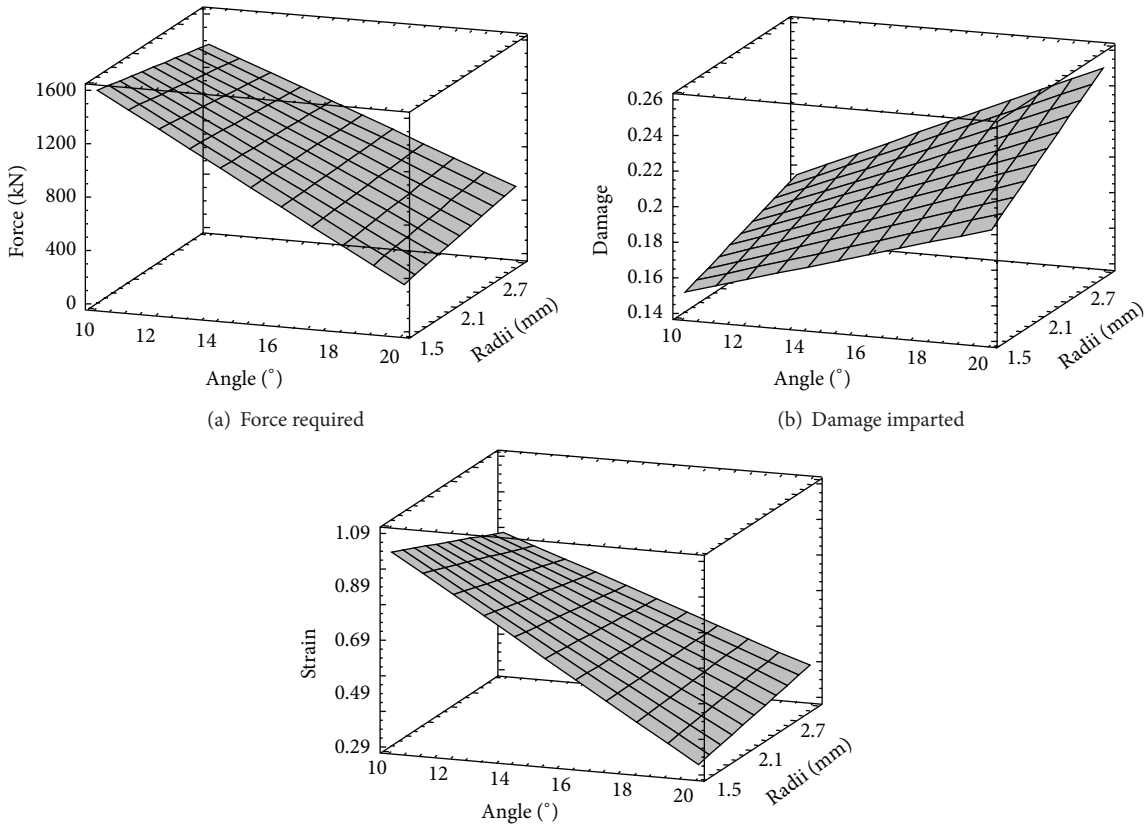

(a) Force required

(b) Damage imparted

(c) Strain

Figure 4: Estimated response surfaces.

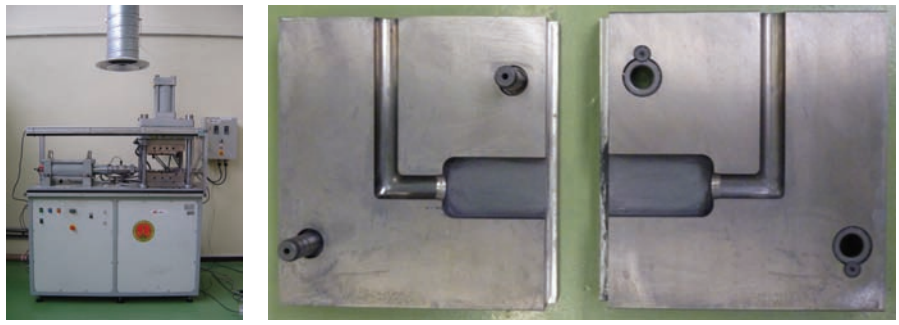

(a) ECAE hydraulic press

(b) ECAE dies employed

Figure 5: ECAE hydraulic press and dies employed.

considering the zone in contact with the billet and the fillet radii. With the aim of modelling the material behaviour as precisely as possible, flow rules obtained from isothermal compression tests of AA5083 billets (16 mm in length and 8 mm in diameter) are used. Moreover, artificial neural networks (ANNs) are employed so as to generate them from experimental data. In all the simulations, an isotropic material with a Young's modulus of 70 GPa and a Poisson's coefficient of 0.3 has been considered for the billet.

The friction model employed is shear type, which is recommended for forging applications, and the friction coefficient taken is 0.5. With these simulations, it is possible to obtain the force required for the forging, the strain and the damage values, the temperature evolution during the process, and the stress values in the dies, which will be outlined in the following sections.

With the aim of assessing the accuracy for the performed simulations, their force results are compared with those real values obtained for the experimental tests under the same conditions of temperature, forging velocity, die geometry, and material employed. Figure 8 shows the precision of the FEM simulations with respect to the prediction of the force in

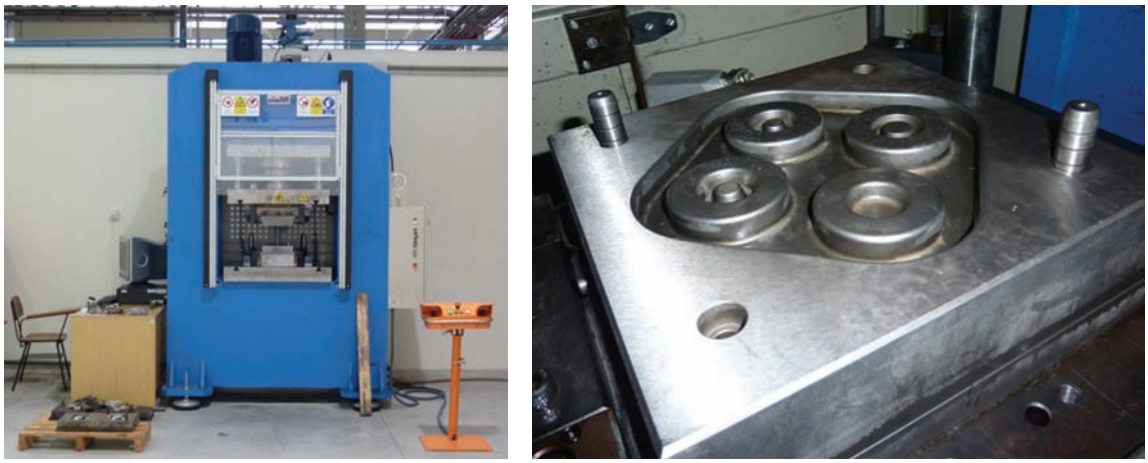

(a) Hydraulic press (b) Dies manufactured

Figure 6: Equipment employed for the isothermal forging.

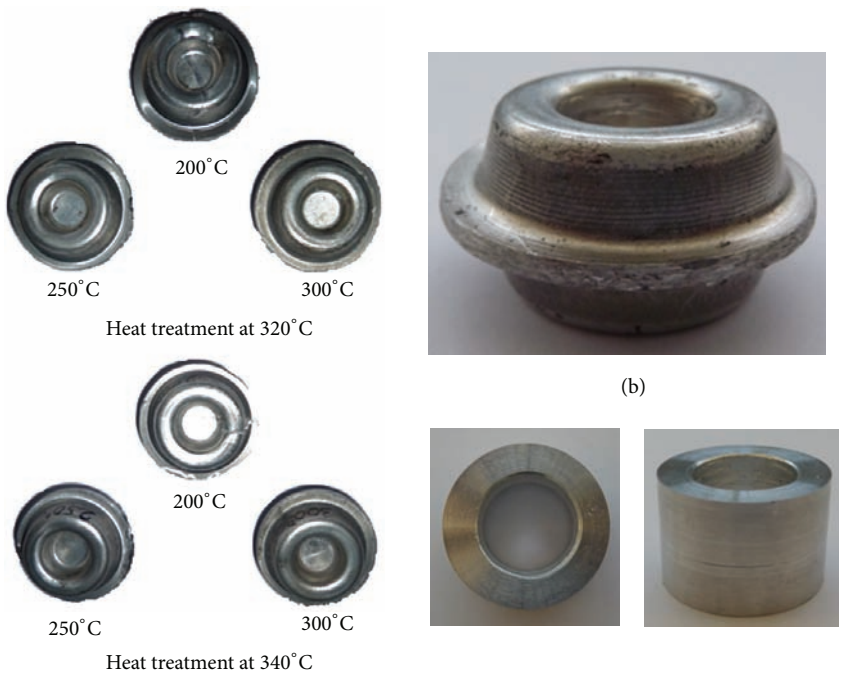

Figure 7: Samples of nanostructured rings. (a) Samples studied. (b) Sample before machining. (c) Final machining.

the real tests for the case of the isothermal forging at 200°C, 250°C, and 300°C and the decrease of the FEM simulation force when temperature is increased.

The curves consist of a first part with a constant force value and a subsequent exponential increase which takes place when the flash starts to generate and the surface to be deformed is higher. This behaviour is more pronounced in the FEM simulations. Moreover, the force value in the simulations remains slightly lower than the force value in the real tests during the stabilisation stage, and it remains slightly higher in the stage where the exponential increase happens. Nevertheless, the FEM simulations agree reasonably well with the real tests, and thus the obtained results may be considered correct and accurate. Figure 9 shows the strain achieved in the preform and in the final ring for the forging at 250°C.

The damage has been studied using Crockroft-Latham's model. The accumulated damage increases in the preform and in the ring when we move towards the centre following a radial direction, as can be observed in Figure 10. Taking the ring subsequent machining into account is also important and in this way the most damaged zones are removed.

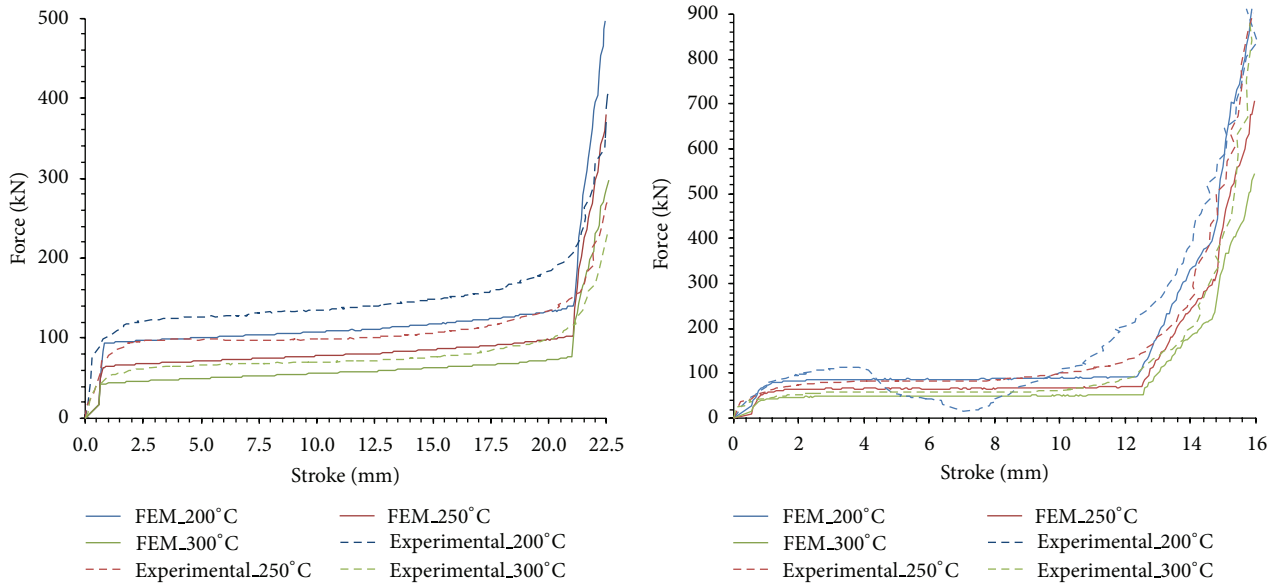

(a) Preform forging (b) Ring forging

Figure 8: Comparison between the experimental and the simulated load stroke curves.

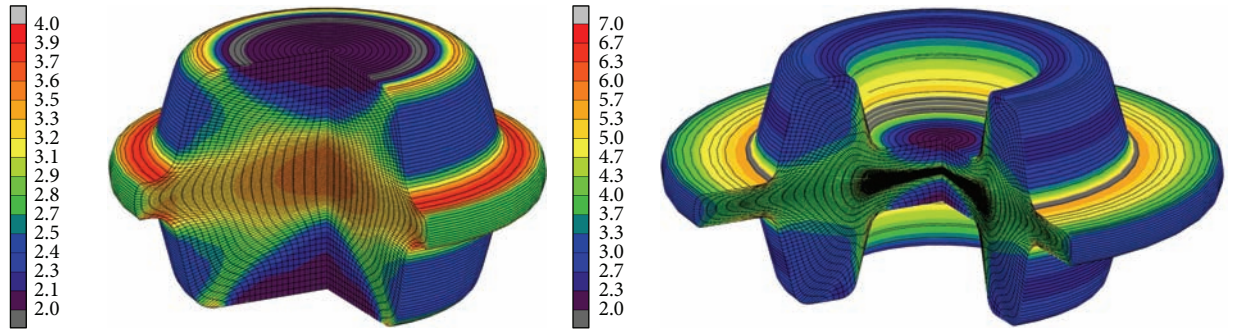

(a) Preform forging (b) Ring forging

Figure 9: Accumulated strain in the material at the end of each isothermal forging stage at 250°C.

The maximum values within the useful zone are 0.15 for the preform and 0.25 for the ring.

Lastly, Figure 11 shows the Von Mises stress values both in the dies and in the billet at the final step of the forging process of the preform and the ring. In the case of the forged material, the flow stress corresponds to the Von Mises stress in each calculation step, and it is practically constant along the billet. The Von Mises stress turns out to be more interesting in the case of the dies. The stress values originated within the die should be reduced so as to decrease its wear and avoid plastic deformations which would modify the final shape of the ring in the consecutive forging processes. The highest stress values are located at the inner fillet radii of the die cavity, and they are higher when these fillet radii are diminished.

When increasing temperature, a reduction in the Von Mises stress values of the dies occurs due to the lower flow stress of the deformed material.

4. Analysis of Mechanical Properties and Microstructure

Once the die has been manufactured and the isothermal forging tests of the ring have been carried out, a study on the part microhardness and the force required for the process is made as well as a microstructure analysis by means of scanning electron microscopy (SEM). As was previously mentioned, the forging process was carried out at temperature values of 200°C, 250°C, and 300°C with a press constant velocity of 50 mm/min. The ECAE processed material was forged both with no subsequent heat treatment and after having been subjected to a heat treatment which consisted of increasing the temperature up to 340°C at a heating rate of 12°C/min and a subsequent cooling in water.

4.1. Microhardness of the Samples. As was shown in the previous section, the rings present a central zone with

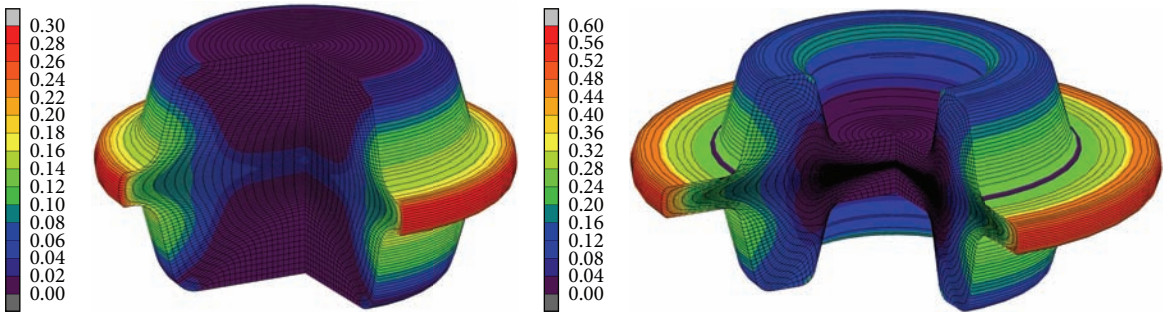

(a) Preform forging (b) Ring forging

Figure 10: Damage imparted to the material at the end of each isothermal forging stage at 250°C.

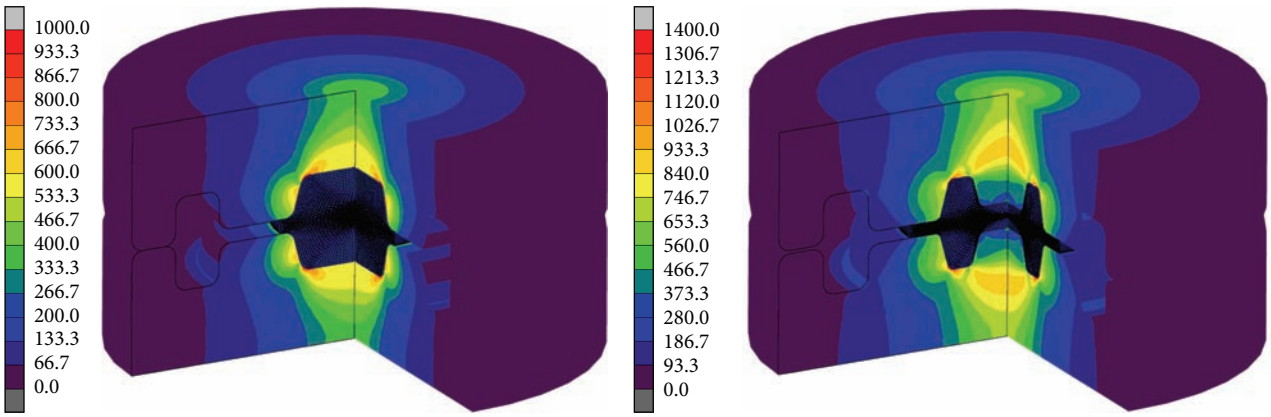

(a) Preform forging (b) Ring forging

Figure 11: Von Mises stress values in the dies and in the billet at the end of each isothermal forging stage at 250°C.

Table 3: Microhardness for the AA5083 samples prior to isothermal forging, where N0 represents the AA5083 initial material, N2 the ECAE processed AA5083 and N2 TT 340°C the ECAE processed AA5083 with the subsequent heat treatment at 340°C.

	N0	N2	N2 TT 340°C
	87.3	123.7	106.2
	83.2	140.6	98.2
	86.3	142.4	112.7
	76.0	154.8	103.0
	87.4	140.4	103.7
Mean	84.04	140.38	104.76
Standard deviation	4.81	11.07	5.30

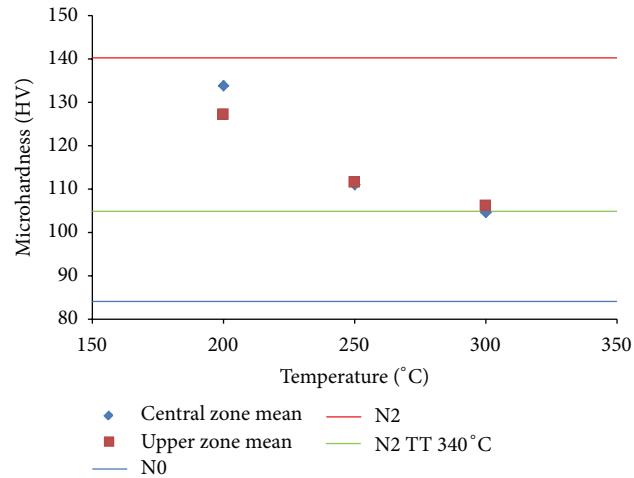

Figure 12: Microhardness mean values at the zones selected in the ring.

a higher strain values than that accumulated in the upper and bottom zones. Due to the different accumulated strain value in these ring zones, microhardness tests are carried out at two different zones: central zone and upper zone.

The samples selected for the study of microhardness were those for the heat treatment at 340°C due to the fact that there were no cracks in the rings. After being cut into sections of 8 mm × 12 mm, they were embedded in resin and polished. Subsequently, ten microhardness measurements were taken per sample, where five of them correspond to the central zone of the ring and the other five correspond to the upper zone of it. Table 3 shows the microhardness values of the material before the isothermal forging whereas Table 4 shows the results obtained for these measurements after the isothermal forging.

Table 4: Microhardness for the material samples after the ring isothermal forging.

Position	200°C		250°C		300°C	
	Central zone	Upper zone	Central zone	Upper zone	Central zone	Upper zone
(0,0)	131.5	124.1	109.3	107.8	95.6	108.3
(0,1)	131.1	129.2	110.1	119.8	105.0	106.9
(0,2)	137.7	128.9	110.2	113.3	105.7	105.5
(0,3)	132.2	126.0	112.3	107.2	105.2	101.0
(0,4)	136.6	127.4	112.8	110.0	111.5	108.7
Mean	133.82	127.12	110.94	111.62	104.60	106.08
Standard deviation	3.09	2.12	1.52	5.16	5.71	3.11

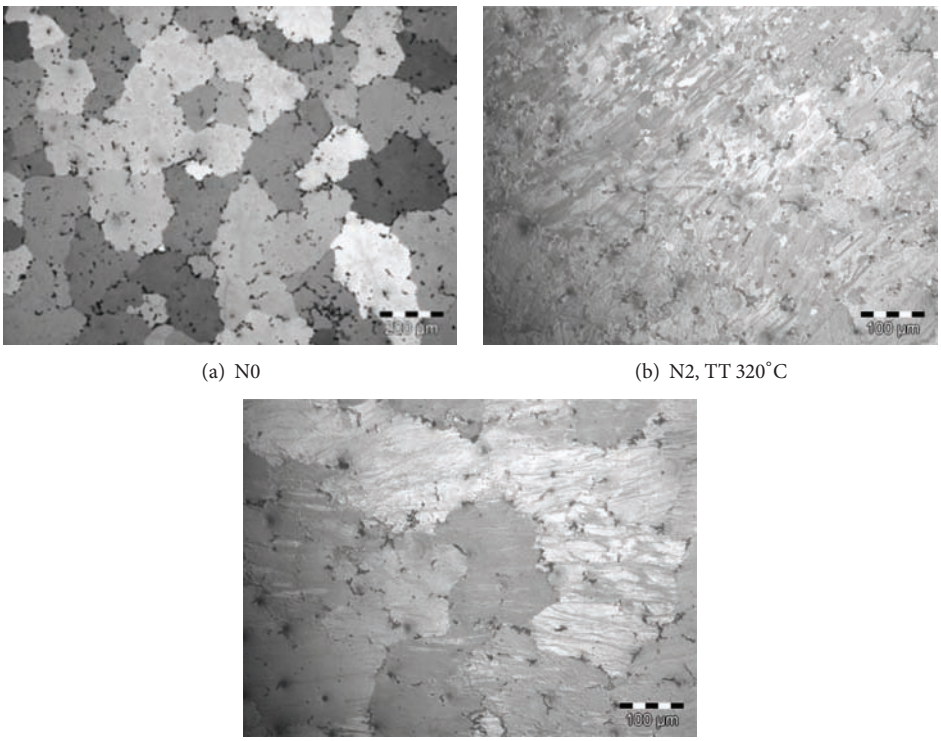

(a) N0

(b) N2, TT 320°C

(c) N2, TT 340°C

Figure 13: Microstructure of the AA5083.

With respect to the starting material, an increase of 64% in hardness between this N0 and the ECAE processed material (N2) can be observed in Figure 12. After the heat treatment enabling the forging process in the ring with no cracks, the microhardness decreases by 25%, but it continues being 24% higher than the N0 state. After carrying out the isothermal forging of the rings, an increase in the material hardness is observed except in the case of the forging at 300°C. In the case of the forging at 200°C, the microhardness is increased to a maximum of 24% in relation to the heat-treated material to be forged, and it is observed that the hardness is higher at the ring upper zone. This validates the strain results obtained in the simulations. In the case of forging at 250°C, the hardness obtained is 5% higher than the initial one, and there are no significant differences between the ring different zones.

4.2. Discussion of Microstructure Results. The microstructure of the samples is analysed so as to verify a possible excessive grain growth, to observe deformation bands and to confirm the existence of submicrometric grains. Figure 13 shows the AA5083 microstructure in annealed state and after having been ECAE processed. The annealed initial material presents a grain size of approximately 200 μm. When it is ECAE processed twice with route C, deformation bands appear even after having been subjected to the two heat treatments under consideration.

As pointed out by El-Danaf [24], it is reasonable to expect, in advance, that after the two ECAE passages, the microstructure will be mainly composed of low angle grain boundaries (LAGBs), whose properties are a function of the misorientation. Nevertheless, it is also expected that, because of the subsequent forging process, these LAGBs will

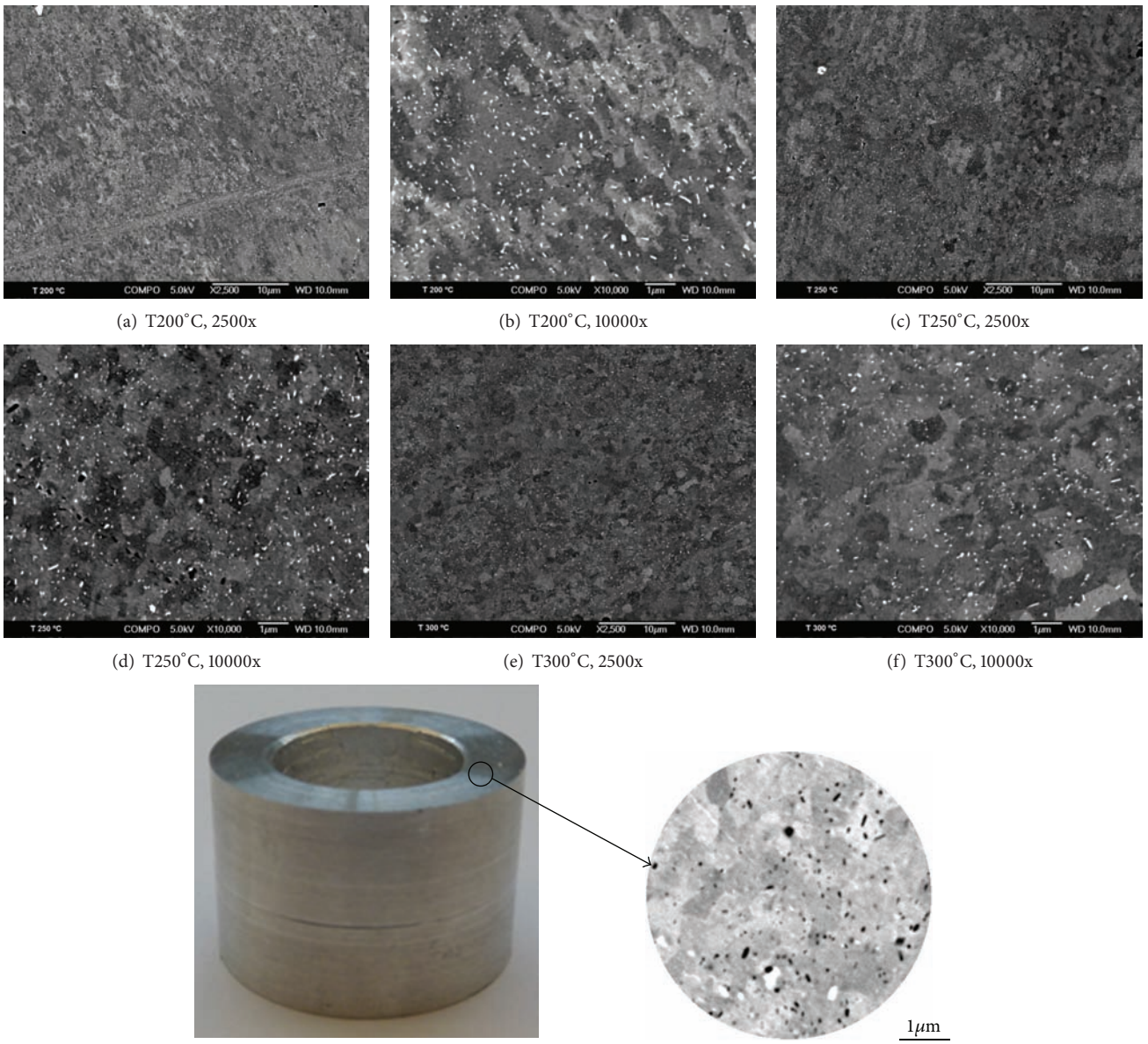

(a) T200°C, 2500x (b) T200°C, 10000x (c) T250°C, 2500x

(d) T250°C, 10000x (e) T300°C, 2500x (f) T300°C, 10000x

(g) Ring manufactured

Figure 14: Microstructure of the rings manufactured by isothermal forging at different temperature values from predeformed material.

be transformed into high angle grain boundaries (HAGBs). On the other hand, in the recent review technical paper on grain boundaries in ultrafine grained materials, carried out by Sauvage et al. [25], these grain boundaries are mainly characterised by an excess of grain boundary energy and the presence of both long range elastic stresses and enhanced free volumes, which may be considered to be the present case.

As can be observed in Figure 14, the samples forged at 200°C and 250°C possess deformation bands caused both by the isothermal forging and by the previous ECAE processing. In the case of the sample forged at 250°C, already recrystallized zones are observed combined with these deformation bands. Nevertheless, the sample forged at 300°C does not present this type of deformations, and it may be observed that the grain size is higher than that in other samples, where this causes a decrease in hardness and worse mechanical properties. Furthermore, a submicrometric grain size is observed in the samples forged at a lower temperature value.

Due to the existence of different precipitates in the samples, a study for the case of the ring forged at room temperature is made by energy dispersive X-ray spectroscopy (EDX) with the aim of determining the chemical composition of the existing precipitates. Figure 15 shows the zones where the analyses were taken and their corresponding EDX spectra. It can be observed that the matrix is mainly composed of aluminium and magnesium, whereas the precipitates are composed of manganese, magnesium, iron, and silicon.

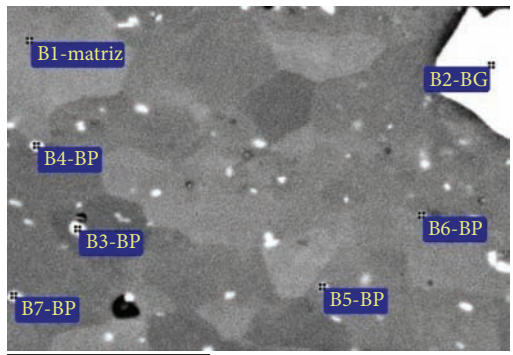

(a)

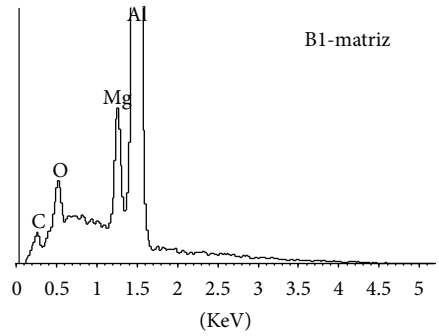

Full scale 1350 cts cursor: 0.035 (937 cts)

(b)

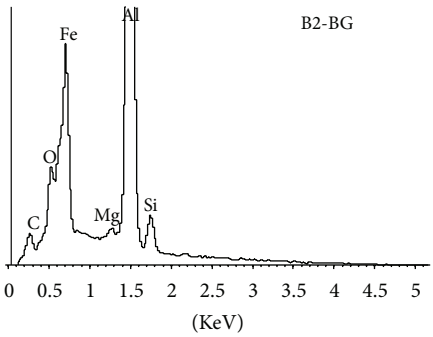

Full scale 1948 cts cursor: 0.035 (906 cts)

(c)

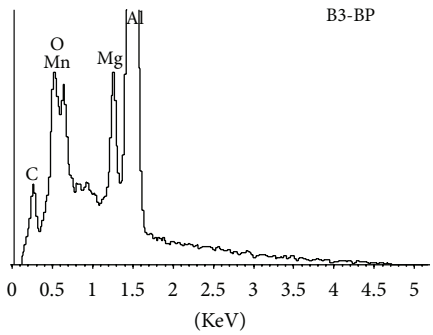

Full scale 815 cts cursor: 0.023 (2476 cts)

(d)

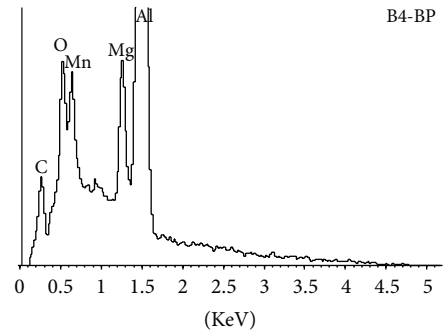

Full scale 815 cts cursor: 0.023 (2495 cts)

(e)

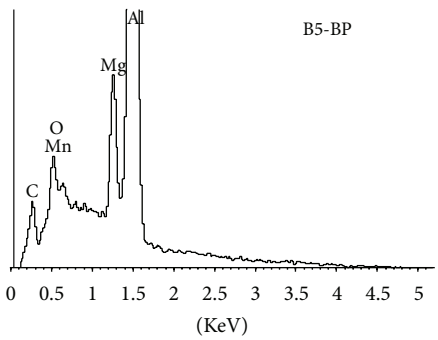

Full scale 1033 cts cursor: 0.035 (931 cts)

(f)

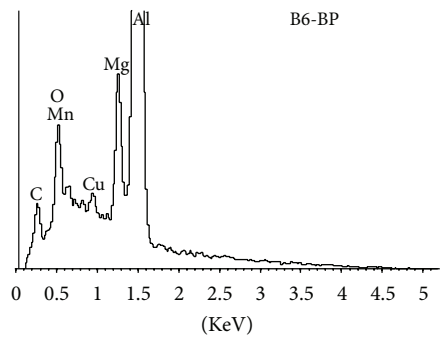

Full scale 1033 cts cursor: 0.035 (900 cts)

(g)

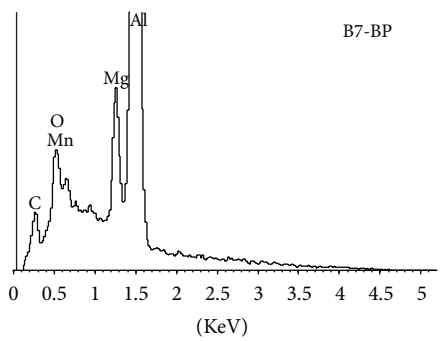

Full scale 1033 cts cursor: 0.035 (921 cts)

(h)

Figure 15: Chemical composition (EDX spectra) of both the matrix and the precipitates for the AA5083 samples.

5. Conclusions

In this research work, it has been demonstrated that it is possible to manufacture rings with submicrometric microstructure from the isothermal forging of previously ECAE processed materials. The optimal geometrical parameters of the forging dies for manufacturing the rings have been selected by using FEM simulations along with design of experiments.

It has been found that the rings manufactured by isothermal forging at 200°C have the microhardness highest values for all the studied cases, but when forging at this temperature, cracks appear in the forged parts. The lowest processing force value takes place in the isothermal forging at 300°C. The optimum forging temperature turns out to be 250°C. Previous to the isothermal forging of the rings at 250°C, the ECAE processed AA5083 is subjected to a heat treatment which consists of increasing its temperature from 25°C to 340°C at a heating rate of 12°C/min. Under these conditions, a compromise solution is achieved in such a way that we are able to obtain a lower isothermal forging force, an intermediate microhardness value due to the presence of deformation bands combined with zones starting to recrystallize, and an optimum state of the nanostructured ring obtained due to a lack of cracks.

Acknowledgment

The authors acknowledge the support given by the Spanish "Ministry of Science and and Innovation" (now "Ministry of Economy and Competitiveness") through the Research Project DPI2010-18941.

References

[1] R. Z. Valiev and T. G. Langdon, "Principles of equal-channel angular pressing as a processing tool for grain refinement," *Progress in Materials Science*, vol. 51, no. 7, pp. 881–981, 2006.

[2] T. G. Langdon, "The principles of grain refinement in equal-channel angular pressing," *Materials Science and Engineering A*, vol. 462, no. 1-2, pp. 3–11, 2007.

[3] V. M. Segal, "Equal channel angular extrusion: from macromechanics to structure formation," *Materials Science and Engineering A*, vol. 271, no. 1-2, pp. 322–333, 1999.

[4] Y. Iwahashi, J. Wang, Z. Horita, M. Nemoto, and T. G. Langdon, "Principle of equal-channel angular pressing for the processing of ultra-fine grained materials," *Scripta Materialia*, vol. 35, no. 2, pp. 143–146, 1996.

[5] C. J. Luis Pérez, "On the correct selection of the channel die in ECAP processes," *Scripta Materialia*, vol. 50, no. 3, pp. 387–393, 2004.

[6] B. Huarte, C. J. Luis, I. Puertas, J. León, and R. Luri, "Optical and mechanical properties of an Al-Mg alloy processed by ECAE," *Journal of Materials Processing Technology*, vol. 162-163, pp. 317–326, 2005.

[7] R. Kapoor and J. K. Chakravartty, "Deformation behavior of an ultrafine-grained Al-Mg alloy produced by equal-channel angular pressing," *Acta Materialia*, vol. 55, no. 16, pp. 5408–5418, 2007.

[8] M. D. Sangid, G. J. Pataky, H. Sehitoglu, R. G. Rateick, T. Niendorf, and H. J. Maier, "Superior fatigue crack growth resistance, irreversibility, and fatigue crack growth-microstructure relationship of nanocrystalline alloys," *Acta Materialia*, vol. 59, no. 19, pp. 7340–7355, 2011.

[9] Y. T. Zhu, T. C. Lowe, and T. G. Langdon, "Performance and applications of nanostructured materials produced by severe plastic deformation," *Scripta Materialia*, vol. 51, no. 8, pp. 825–830, 2004.

[10] S. Ferrasse, V. M. Segal, F. Alford, J. Kardokus, and S. Strothers, "Scale up and application of equal-channel angular extrusion for the electronics and aerospace industries," *Materials Science and Engineering A*, vol. 493, no. 1-2, pp. 130–140, 2008.

[11] S. Poortmans, L. Duchêne, A. M. Habraken, and B. Verlinden, "Modelling compression tests on aluminium produced by equal channel angular extrusion," *Acta Materialia*, vol. 57, no. 6, pp. 1821–1830, 2009.

[12] A. S. M. Agena, "A study of flow characteristics of nanostructured Al-6082 alloy produced by ECAP under upsetting test," *Journal of Materials Processing Technology*, vol. 209, no. 2, pp. 856–863, 2009.

[13] C. J. Luis-Pérez, I. Puertas, D. Salcedo, J. León, and I. Pérez, "Comparison between FEM and experimental results in the upsetting of nano-structured materials," *Materials Science Forum*, vol. 713, pp. 31–36, 2012.

[14] Y. G. Jin, H. M. Baek, Y.-T. Im, and B. C. Jeon, "Continuous ECAP process design for manufacturing a microstructure-refined bolt," *Materials Science and Engineering A*, vol. 530, no. 1, pp. 462–468, 2011.

[15] J. S. Choi, S. Nawaz, S. K. Hwang, H. C. Lee, and Y. T. Im, "Forgeability of ultra-fine grained aluminum alloy for bolt forming," *International Journal of Mechanical Sciences*, vol. 52, no. 10, pp. 1269–1276, 2010.

[16] A. Yanagida, K. Joko, and A. Azushima, "Formability of steels subjected to cold ECAE process," *Journal of Materials Processing Technology*, vol. 201, no. 1–3, pp. 390–394, 2008.

[17] P. K. Chaudhury, B. Cherukuri, and R. Srinivasan, "Scaling up of equal-channel angular pressing and its effect on mechanical properties, microstructure, and hot workability of AA 6061," *Materials Science and Engineering A*, vol. 410-411, pp. 316–318, 2005.

[18] J. H. Lee, S. H. Kang, and D. Y. Yang, "Novel forging technology of a magnesium alloy impeller with twisted blades of micro-thickness," *CIRP Annals*, vol. 57, no. 1, pp. 261–264, 2008.

[19] I. Puertas, C. J. Luis Pérez, D. Salcedo, J. León, J. P. Fuertes, and R. Luri, "Design and mechanical property analysis of AA1050 turbine blades manufactured by equal channel angular extrusion and isothermal forging," *Materials and Design*, vol. 52, pp. 774–784, 2013.

[20] T. Altan, G. Ngaile, and G. Shen, *Cold and Hot Forging: Fundamentals and Applications*, ASM International, Materials Park, Ohio, USA, 2005.

[21] K. H. Jung, D. K. Kim, Y. T. Im, and Y. S. Lee, "Prediction of the effects of hardening and texture heterogeneities by finite element analysis based on the Taylor model," *International Journal of Plasticity*, vol. 42, pp. 120–140, 2013.

[22] D. Salcedo, C. J. Luis-Pérez, J. León, R. Luri, and I. Puertas, "A method for obtaining spur gears from nanostructured materials," *Advanced Materials Research*, vol. 498, pp. 7–12, 2012.

[23] C. J. Luis, D. Salcedo, J. León, R. Luri, I. Puertas, and J. P. Fuertes, "Procedimiento de fabricación de elementos

mecánicos de geometría hueca con estructura submicrométrica o nanométrica," Número de solicitud: P201330404, Fecha de recepción: 20/03/2013, Oficina receptora: OEPM Madrid, Patent Pending.

[24] E. A. El-Danaf, "Mechanical properties, microstructure and texture of single pass equal channel angular pressed 1050, 5083, 6082 and 7010 aluminum alloys with different dies," *Materials and Design*, vol. 32, no. 7, pp. 3838–3853, 2011.

[25] X. Sauvage, G. Wilde, S. V. Divinski, Z. Horita, and R. Z. Valiev, "Grain boundaries in ultrafine grained materials processed by severe plastic deformation and related phenomena," *Materials Science and Engineering A*, vol. 540, pp. 1–12, 2012.